이학석사 학위논문

Two dominant types of heat waves in South Korea: the circumglobal teleconnection (CGT) and warm advection

우리나라 폭염의 두 가지 발생 요인: CGT유형과 온난이류 유형

2019년 8월

서울대학교 대학원

지구환경과학부

정 지 영

Two dominant types of heat waves in South Korea: the circumglobal teleconnection (CGT) and warm advection

우리나라 폭염의 두 가지 발생 요인: CGT유형과 온난이류 유형

지도 교수 허 창 회

이 논문을 이학석사 학위논문으로 제출함
2019년 8월

서울대학교 대학원
지구환경과학부
정 지 영

정지영의 이학석사 학위논문을 인준함
2019년 8월

위 원 장 김 광 열 (인)

부위원장 허 창 회 (인)

위 원 백 종 진 (인)

Abstract

Two dominant types of heat waves were determined through analysis of extreme heatwave cases in South Korea. Four years (1994, 2013, 2016 and 2018) of the extreme heat were extracted since 1973, in which heat wave days are more than one standard deviation (6.9 days) above average (10.6 days). The first type to which 1994 and 2018 cases belong is the circumglobal teleconnection (CGT) type. The CGT type makes the heat waves severe starting from July. The analysis on circumglobal geopotential height anomaly presents that, in those two years, the series of high geopotential height anomalies are located around the globe in the mid-latitudes (i.e., circumglobal teleconnection (CGT) patterns), retarding the zonal atmospheric wind speed. In addition, the barotropic high pressure system, which is strongly located in South Korea, would be linked to the early withdrawal of Changma. The second type, to which 2013 and 2016 cases belong is the warm advection type in which heat waves start and last throughout August. This type is related with a low-pressure anomaly in the lower troposphere of South Korea. The analysis on the temperature advection from the surroundings shows that the positive heat advection from Mongolia or Eastern China might serve as the source of both the low-pressure anomaly and warm temperature anomaly in South Korea. Finally, the extreme heat waves frequency in the future climate is assessed by analyzing previously described

atmospheric features in RCP8.5 scenarios. According to the assessment, first, the occurrence of CGT patterns increases in the mid-latitude Northern Hemisphere at the end of twenty first century, and its correlation with the heat wave intensity in South Korea becomes stronger. Second, the frequency of heat advection from the vicinity of South Korea are projected to decrease toward the late of twenty-first century. That is, extreme heat waves events similar to that of 1994 and 2018 are likely to increase while those similar to that of 2013 and 2016 are likely to decrease. Therefore, the extreme heat waves starting in July, which is related with stagnant high-pressure system in the troposphere, seems to be a major concern in South Korea at the end of twenty-first century, rather than that starting in August by heat advection effects.

Keyword : heatwave, circumglobal teleconnection pattern, warm advection, climate change, RCP 8.5 scenario

Student Number : 2017-27486

Table of Contents

List of Tables

List of Figures

1. Introduction

In 2018, a strong, long-lasting heat wave with very high surface temperatures was observed in South Korea (KMA, 2018). The daily maximum temperature in Seoul, the capital of South Korea, is 39.6° C as a city record, and for Hongcheon, a county in Gangwon Province in South Korea, is 41.0° C as a national record. The intense heat waves lasted for about 31 days, which broke the record set in 1973. The number of heat illness reached about 4,300 and the number of heat-related deaths reached 48 (total death toll is more than 7000), reported by Korea Centers for Disease Control and Prevention. This severe heat wave did not occur only in 2018. The second extreme case in the last 40 years occurred in 1994, in which daily maximum temperature exceeded 35° C for over 30 days. There were 92 heat-related deaths, with the total death toll exceeding 3000 in South Korea (Kysely and Kim, 2009). Moreover, 2013 and 2016 was the fourth and third-hottest year on record since 1973, respectively. As the numbers show, it is necessary to analyze the characteristics of heat waves as it is an enormous danger to human health (Amengual et al., 2014; Lee et al., 2016), ecosystems (Beniston et al., 2007) and damage to crop production (Kim et al., 2010; Zuo et al., 2015).

Previous studies on heat waves of South Korea were conducted by analyzing the patterns of heat wave of a particular year, by researching the overall pattern in East Asia, or by enlarging the

research boundaries to the entire Northern Hemisphere. Examples of researching the pattern of a particular year include the following. First, Yeh et al. (2018) analyzed the dynamical processes of heat waves in 2016 over South Korea, which occurred due to the anomalous high geopotential height around the Mongolia and the Kamchatka Peninsula. Second, Min et al. (2014) assessed the possible long-term impacts of increased greenhouse gas on increase of summer temperatures of South Korea, especially the extreme 2013 event. Third, Yoo et al. (2004) explained the rise in 1994 of East and Southeast Asia by the ocean-atmosphere coupling of the extratropical Pacific. By comparing the case to that of 1993, the increase in tropical sea surface temperature (SST) played a role in summer temperature. In addition, there are researches on the trend of overall East Asia. Xu et al. (2019) examined the large-scale circulation anomalies associated with an anomalous anticyclone in July and August over East Asia, which suggests that wave trains propagate eastward along the Asian westerly jet in the upper troposphere. Some research the heat wave on a larger scope. Lee and Lee (2016) analyzed the interannual variation of heat wave frequency in South Korea and examined its connection with large-scale atmospheric circulation. As these examples show, there has been an extensive research on the heat waves in South Korea. As past studies focused on the overall patterns, our study focused on analyzing the commonalities and differences of extreme heat wave cases to identify the characteristics of the severe cases in South

Korea.

Many climatic factors directly or indirectly affect the climatological features of the Northern Hemisphere countries, which makes extreme cases more moderate or intense. Potential climate factors to affect summer extreme temperature in the Northern Hemisphere are the following: El Niño–Southern Oscillation (ENSO) (e.g. Wang et al., 2009), the Indian summer monsoon (ISM) and the western North Pacific summer monsoon (WNPSM) (e.g. Sui et al., 2007; Lee et al., 2013; Wu, 2017; Chen et al., 2019), the North Pacific SST variability (e.g. Lau et al., 2004; Ham et al., 2016), the Arctic Oscillation (AO) (e.g. Thompson and Wallace, 2000; Lhotka and Kysely, 2015), the circumglobal teleconnection (CGT) (e.g. Ding and Wang, 2005; Lee et al., 2011; Beverley et al., 2019), tropical cyclone activity in the western North Pacific (e.g. Sovel and Camargo, 2005), and Tibetan plateau (e.g. Duan and Wu, 2005; Wang et al., 2008) (Ha et al., 2012). Those factors can change the extreme heat events with interaction with one another.

Past researchers were able to relate the factors with the varying summer temperatures but there has not been a research to find common factors of extreme cases. Therefore, this study distinguished two types by investigating the dominant causes of extreme heat wave cases (in 1994, 2013, 2016 and 2018) in South Korea. We also examined how two types would change in the future projection if greenhouse gas emissions maintain current growth trends. The dissertation is organized as the following. Section 2

presents data and methods that used in this dissertation. Section 3 describes the current status and possible causes of the heat wave in South Korea. Section 4 show two types of extreme heat wave cases. Section 5 shows variation of two types in future projection with RCP8.5 scenario. Section 6 summarizes and discusses the results in Section 3, 4 and 5.

2. Data and Methods

2.1 Data

The daily mean and maximum surface air temperatures from 45 Automated Synoptic Observing System (ASOS) weather stations in South Korea for 1973–2018 were obtained from the Korea Meteorological Administration (KMA). We used the Changma retreat dates announced by the KMA. In addition, the daily geopotential height, zonal and meridional winds, 2m temperatures, total precipitation, and specific humidity were obtained from the European Centre for Medium-Range Weather Forecasts Re-Analysis (ERA)-interim with 0.75° × 0.75° resolution for 1979–2018. We used the Arctic Oscillation (AO) index, one of the possible climate factors. This index is produced by the National Oceanic and Atmospheric Administration Climate Prediction Center which is publicly provided from their web site. For future projection, the representative concentration pathway (RCP) 8.5 scenario, produced by a multi-member Community Earth System Model version 1 (CESM1) Community Atmosphere Model, version 5 (CAM5), is used. RCP8.5 describes a very high greenhouse gas emission scenario with radiative forcing at 8.5 W/m^2 by 2100. The spatial resolution of the climate model is 0.9375° latitude by 1.25° longitude.

2.2 Methods

There are many of definitions of heatwaves in literature, such as heatwave duration index, Expert Team on Climate Change Detection, Monitoring and Indices (ETCCDI), and etc. (Frich et al., 2002; Meehl and Tebaldi, 2004; Alexander et al., 2006). This paper uses the definition of heat wave adopted by KMA. Heatwave day (HWD) is defined as an average of the number of day when the maximum temperature exceeds 33° C at each ASOS stations (Lee and Lee, 2016; Yeh et al., 2018; Xu et al., 2019). The threshold is set at 33° C as this temperature has an important meaning in human health (Kyselý and Kim, 2009). The intensity of the heat waves (HWI) is defined as the average of the top 10% of the daily summer temperature since there is a correlation between daily mean temperature and heat wave days. In grid data, the average of the values in Korean Peninsula (KP) region is used. The KP region is defined as the smallest box that can contain all 45 ASOS stations (Fig. 1a).

The CGT, first identified by Ding and Wang (2005), has a major role in modulating the observed weather pattern in the Northern Hemisphere. The CGT index is defined by the 200-hPa geopotential height averaged over the north western India (35° - 40° N, 60° -70° E; Ding and Wang, 2005). This CGT index does not account for anticyclonic anomalies over East Asia. Therefore, by adding the geopotential height anomalies of two regions (the

D&W area referred by Ding and Wang, and EA area in Table 1), a newly defined CGT index (CGTI) is used in this paper. Table 1 lists the five anomalies of high geopotential height when CGT pattern is present. These points include North Pacific, North America, Europe regions, as well as the two regions mentioned above. These points were chosen by altering the points set by Beverley et al. (2019). Also, these point do not only have a positive correlation with the D & W area, but also with other chosen points of high geopotential height.

To evaluate possible climate factors related to heat waves, we used several climate indices as the following. The WNPSM (western North Pacific summer monsoon) index (WNPSMI) is defined as a difference of 850-hPa westerlies between the south of the western North Pacific (5° -15° N, 100° -130° E) and the north of the western North Pacific (20° -30° N, 110° -140° E) during JJA. Likewise, the ISM index (ISMI) is defined as difference of 850-hPa westerlies between a region north of the Indian Ocean (5° -15° N, 40° -80° E) and a region north of India (20° -30° N, 70° -90° E) (Wang et al., 2001). Western North Pacific subtropical high (WNPSH) is defined as the normalized 850-hPa geopotential height anomalies averaged over the WNPSH region (15° -30° N, 110° - 150° E) (Lee et al., 2013). Oceanic Niño Index (ONI) is defined as 3-month running means of SST anomalies in the Niño 3.4 region (5° N-5° S, 120° -170° W). Bonin high index (BHI) and North Pacific high index (NPHI) are defined as the normalized 500-

hPa geopotential height anomalies averaged over the BH (25° – 30° N, 140° – 145° E) and NPH (27.5° –30° N, 170° – 180° E), respectively (Ha and Lee, 2007).

Figure 1b shows the analysis area set to identify the heat and moisture transported in South Korea. The area is divided into four quadrants and they are numbered in counterclockwise in consistent to plane geometry. The occurrence of the advection of heat or moisture into the KP region is defined as the wind direction. In the first quadrant, existence of advection is defined when both zonal wind and meridional wind are negative. In the second quadrant, existence of advection is defined when zonal wind is positive and meridional wind is negative. In the third quadrant, existence of advection is defined when both zonal wind and meridional wind are positive. In the fourth quadrant, existence of advection is defined when zonal wind is negative and meridional wind is positive.

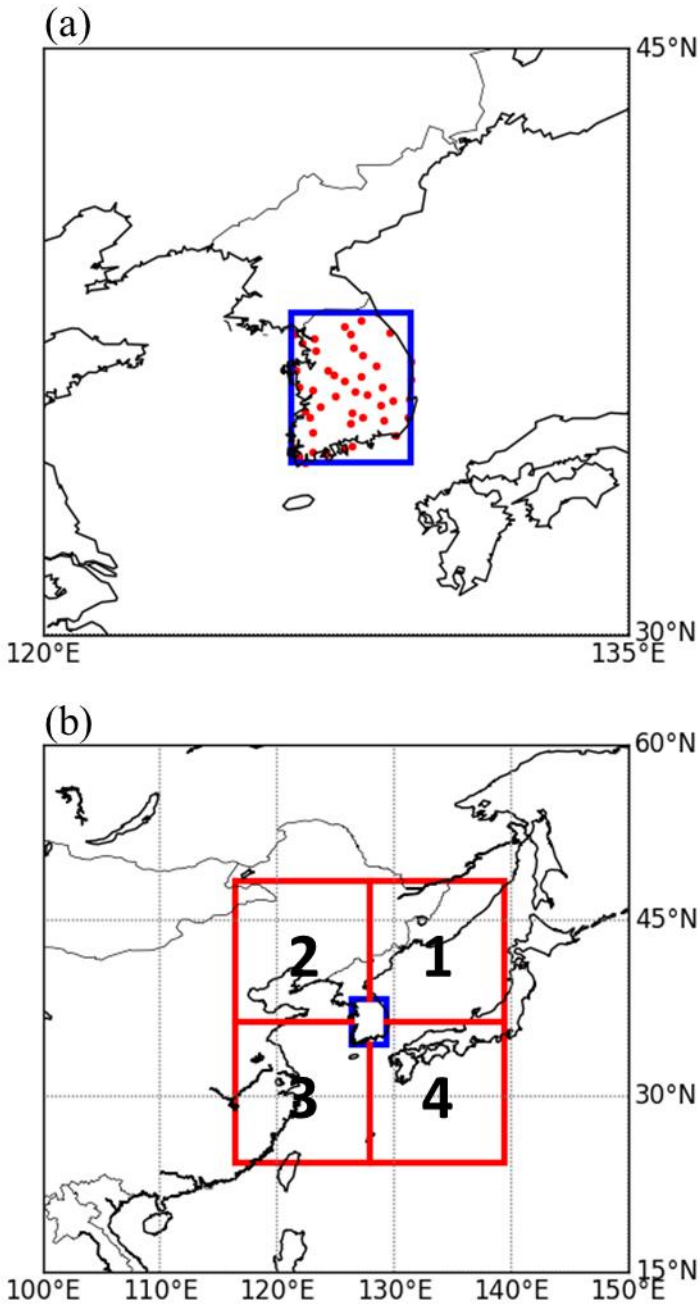

Figure 1. (a) Spatial distribution of the 45 ASOS stations (red dots) in the KP region (blue box). (b) Advection analysis region of our study. The analysis domain to calculate heat and moisture advection outside of the KP region (blue box). The domains are numbered in counterclockwise order.

Table 1. Location of the red boxes in Figure 8. These five locations show high geopotential height when CGT pattern is present.

Region	Abbreviation	Domain
Ding and Wang	D&W	35° −40° N, 60° −70° E
Northwest Europe	NWEUR	45° −65° N, 0° −20° E
East Asia	EA	30° −50° N, 110° −140° E
North Pacific	NAPC	40° −60° N, 170E° −140° W
North America	NAM	40° −60° N, 80° W−50° W

3. Characteristics of heat waves in South Korea

3.1 Past heat waves

Figure 2 shows the monthly number of days of heatwaves in South Korea from 1979 to 2018 in a time series. Colored years, 1994, 2013, 2016, and 2018, present when the number of heatwave days (HWD) are more than one standard deviation above than that of the 40 year (1979–2018) heatwave day mean. Each pattern and color in the bar graph represents the days, yellow (blank), orange (dots) and red (stripes) mean June, July and August, respectively. The percentage of HWD in July 1994 and 2018 were surprisingly greater than that of other months, which means that the heat waves started early. In 2013 and 2016, however, the percentage of the HWD in August was high. The percentage of HWD occurred for each month in the four years is given in Table 2. Compared to the climatic values, the HWD accounts for 61.7% (July 1994), 49.3% (July 2018), 71.1% (August 2013) and 74.8% (August 2016) of the corresponding annual total amount. Since there is a difference in monthly heat waves, it is necessary to check the mechanism separately for each month. Therefore, we conducted a climatological analysis on why the heat waves occurred earlier for cases of 1994 and 2018 but suddenly and later in the cases of August 2013 and 2016.

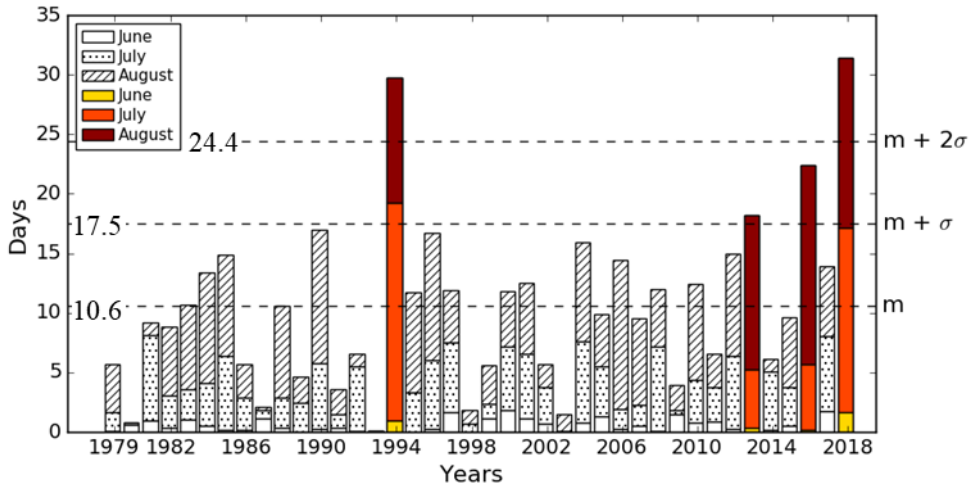

Figure 2. Time series (1979–2018) of the heatwave days in South Korea. Colored bars denote extreme years, in which heatwave days from June to August are more than one standard deviation (6.9 days) above the mean (10.6 days).

Table 2. The number of monthly heatwave days and the percentage. The bold denotes the month with a larger percentage than climatology.

	June	July	August	Total
Climatology	0.6 (5.9%)	4.2 (39.6%)	5.8 (54.5%)	10.6
1994	1.0 (3.2%)	**18.3 (61.7%)**	10.4 (35.1%)	29.7
2013	0.4 (2.0%)	4.9 (27.0%)	**13.0 (71.1%)**	18.2
2016	0.2 (0.8%)	5.5 (24.4%)	**16.7 (74.8%)**	22.4
2018	1.6 (5.2%)	**15.5 (49.3%)**	14.3 (45.5%)	31.4

3.2 Possible climate factors

The relationship between the number of HWD and climate factors associated with heat waves in South Korea is given in Table 3. The first row shows the correlation coefficient (r) between HWD and the climate indices during summer (June to August). Other rows show each index value in each extreme year that is normalized for analysis period of 40 years, excluding the Changma (the rainy season in South Korea) column. There is no index for Changma, therefore Changma retreat date is used as the index. Highly correlated indices ($|r| \geq 0.5$) are CGT, AO, and Changma, and have values of 0.7, 0.53, and −0.53, respectively. Other factors that are not accepted should not be ruled out as they can indirectly interact with other climatic factors to cause an effect to heat waves. However, this paper will only focus on the factors that showed significant statistical correlation with one exception of the ISM index. As the normalized index of ISM are all above 1 and the correlation coefficient (0.46) being very close to the range, this factor will be discussed.

The main climate factors, such as Changma, AO, ISM and CGT, are related to the heat wave in South Korea in the following mechanism. First, the Changma with a negative correlation dissipates heat by spraying a large amount of rain. If the rain lasts longer in summer, the hot days will be less. Figure 3 shows the relationship between the retreat date of Changma and HWD. The

extreme years (1994, 2013, 2016 and 2018) are indicated by blue dots and the others are indicated by the plus sign. In the cases of plus sign years, Changma retreat date has a weak negative correlation (−0.44) with HWD. On the other hand, the negative relationship is stronger even in severe heatwave years (−0.98). Second, Arctic Oscillation is a factor that has a positive correlation with HWD. It is well known to be associated with cold waves in winter, but it is also related to the mid−latitude climate in summer. The high AO index indicates low geopotential height during summer. Hence, the gradient between low and high latitudes increases which causes the meridional winds to be stronger. Then, the jet moves to the north. Third, ISM is another factor that shows a positive correlation with HWD. During the monsoon, the strong convection causes energy propagation in the upper troposphere by condensation. This energy is transferred to the Korean peninsula which induces anticyclonic anomalies in the upper and lower troposphere. These anomalous high induces clear weather, hot and dry atmosphere through an adiabatic compression process, which affects heatwaves in South Korea (Wu, 2017). If this process extends further the mid−latitude, CGT pattern can be seen which is the forth climate factor to be discussed. CGT pattern stabilizes and stagnates the atmosphere in the mid latitude. If the high point is located in East Asia, as the atmosphere is stagnated it will keep the South Korean summers hot for a long time. Therefore, we analyzed the four climate factors that show high correlation with heat waves

in South Korea, focusing on the extreme years.

Table 3. Correlation coefficient between the number of heatwave days (HWD) and several climate factor indices, such as western North Pacific summer monsoon (WNPSM) index, Indian summer monsoon (ISM) index, western North Pacific subtropical high (WNPSH), circumglobal teleconnection (CGT), Oceanic Niño index (ONI), Okhotsk high intensity (OHI), Arctic Oscillation (AO) index, Bonin high (BH) index and North Pacific high (NPH) index, (first row) in the period of 1979–2018 and normalized values of indices in 1994 (second row), 2013 (third row), 2016 (fourth row) and 2018 (fifth row) with the exception of Changma. Changma data represent the actual withdrawal date of Changma.

	WNPSM	ISM	WNPSH	CGT	ONI	OHI	AO	Changma	BH	NPH
Coef. with HWD	0.33	0.46	−0.33	0.70	−0.02	−0.18	0.53	−0.53	−0.20	−0.25
1994	1.05	1.80	−0.68	2.04	0.42	−0.95	2.49	10th Jul.	−1.01	−1.17
2013	−0.58	2.69	0.45	1.57	−0.43	−0.40	0.66	3rd Aug.	−0.37	0.25
2016	−0.34	1.48	0.10	0.74	−0.46	1.01	0.81	23rd Jul.	0.27	−0.02
2018	1.81	1.46	−1.33	2.24	0.34	0.60	1.65	9th Jul.	0.73	0.67

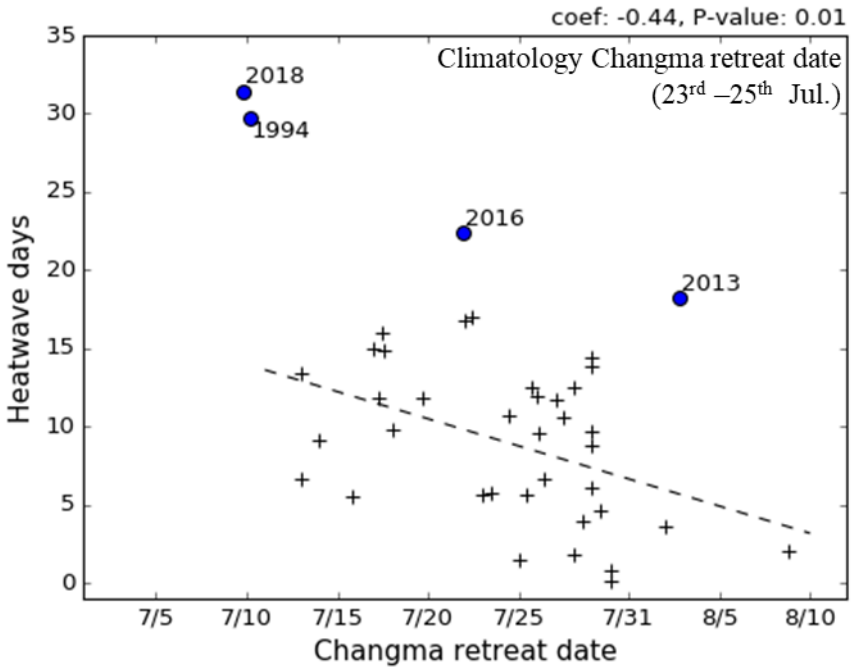

Figure 3. Relationship between Changma retreat date and heatwave days during 1979–2018. The dashed line shows linear fit except for the extreme cases.

4. Separation of extreme heat wave cases

4.1 Circumglobal teleconnection type

To investigate the mechanisms related to heatwaves that occurred in July 1994 and 2018, we examined the withdrawal of rainy season in South Korea. In 1994 and 2018, the rainy season ended quite early, which means that there may be more hot days. The temperature rise after the end of the rainy season is given in Figure 4. Figure 4 shows the daily precipitation anomalies and daily maximum temperatures daily in the extreme summer years. The black dashed line represents the average of the retreat date of Changma observed by 45 ASOS stations. In 1994 (Fig. 4a) and 2018 (Fig. 4d), it only rained a lot in the beginning of July and after that there was only little precipitation and the temperature was much higher than climatology for more than a month. Thus, summer precipitation can affect the heat waves. Therefore, Changma is one possible factor for heat waves in South Korea. The early withdrawal of Changma in 1994 and 2018 can be seen in geopotential height anomaly at 500-hPa (Fig. 5). Figure 5 displays the composite of geopotential height anomalies and winds anomalies at 500-hPa in July. The Changma front is produced between a cold polar air mass (5820 gpm, blue line) and a warm North Pacific high (5880 gpm, red line) (white paper on Changma, 2011). The dashed line represents the climatology and the solid line represents each year.

In 1994 and 2018, the polar air mass line was biased further north than that of climatology. This anomalous high location of the Korean peninsula or the North Pacific high explains the north pushed Changma front (Fig. 5a and d).

For the summer AO index, the normalized values for 1994 and 2018 are 2.49 and 1.65, respectively, which are much higher than the climatology for the analysis period (Table 3). Figure 6 shows the 200-hPa geopotential height anomalies and wind speed in July and August of 1994 and 2018. In July, the geopotential height anomalies over the Arctic in both 1994 and 2018 are negative (Fig. 6a and c). In addition, the jet stream, where the wind speed is over 20 m/s, is located northward compared to climatology (dashed line) on the Korean Peninsula. This is in line with the explanation described in section 3 that as meridional gradient increases, the intensity of wind blowing to the north becomes stronger and the jet stream is shifted to the north. This indicates that the high-pressure system located in South Korea, would not be able to escape easily due to the weakening of the westerlies. In August 1994, geopotential height over the Arctic is weaker than that of July, but the jet stream still passes north of the Korean peninsula (Fig. 6b). In August 2018, there is a dipole pattern over the Arctic, and the location of the jet stream shifts southward than July (Fig. 6d).

The normalized ISM index is 1.8 in the year 1994 and 1.46 in the year 2018, indicating that the ISM is stronger than climatology. The composite maps of geopotential height anomalies at 200-hPa

and 850-hPa are shown in Figure 7. In July 1994, it shows negative anomalies at 850-hPa over the east of India and positive anomalies at 200-hPa over the northwest of India (Fig. 7a). Moreover, the positive anomalies over East Asia is an effect of wave propagation from upper troposphere, mid latitudes continental Asia. This shows a similar pattern to a previous study (Wu, 2017). In the case of July 2018, the anomalies pattern in the lower and upper layers are similar to those of the previous studies although the negative anomalies in between do not overlap (Fig. 7c). In both years, the energy propagated from the northwest of India induces high pressures in the upper and lower layers on the Korean Peninsula and Japan. Therefore, it can be considered that the barotropic anomalous high located on the Korean Peninsula is related to the Indian monsoon. The anomalous barotropic high over the Korean Peninsula is also present in August 1994 (Fig. 7b). In 2018, the anomalies pattern shifts westward (Fig. 7d).

The CGT wave trains across the mid-latitudes by spreading wave energy, which can also affect the heat wave in 1994 and 2018. Anomalies for 200-hPa geopotential height across the Northern Hemisphere are given in Figure 8. The locations of anomalous high in 1994 and 2018 are very similar to that of the CGT pattern (Figs. 8a and c), but the position of some centers are slightly different. When this pattern appears in the mid-latitude of the Northern Hemisphere during summer, the atmospheric flow stabilizes and stagnates. Therefore, countries with high geopotential height

anomalies can have clearer weather and longer-lasting heatwaves. In August, the positions of CGT centers are slightly shifted, but the wave train still remains in the middle latitude (Fig. 8b and d). The positive anomalies of geopotential height moved to the north in the EA region, to the east in the NAPC and the NAM, and to the south in the NWEUR region in 1994. In 2018, the strength of the CGT was weakened and the upper-level high near EA moved northwestward. The CGT pattern, which lasted until August, resulted in the stagnation of mid-latitude atmospheric flow. This caused the high pressure system to maintain over the Korean peninsula for a long time.

To confirm that CGT stagnates the atmosphere circulation over the Korean Peninsula, 200-hPa zonal and meridional winds anomaly is shown by a scatter plot (Fig. 9). Each axis represents the normalized wind anomalies in KP. When the x-axis (y-axis) value is positive, westerly (north) winds are strong, compared to climatology (1979-2018) and vice versa. In July 1994 and 2018, zonal wind anomalies have strong negative values, indicating that the westerlies over Korean Peninsula are weaken (Fig. 9a). In August, anomalies of wind speed were weaker than the case of July, but the negative anomalies were still low as −1 and −2 in 1994 and 2018, respectively. This proves that the system, westerlies weakening, occurred in July is lasted until August.

Since CGT showed the highest correlation with HWD, we examined the CGTI to calculate the correlation with HWI for 40

years. Figure 10 shows the relationship between CGTI and HWI. The correlation coefficient between CGTI and HWI is 0.67 and p-value is 1.81e-6, which indicated highly significant correlation (Fig. 10a). Thus, the higher 200-hPa geopotential anomaly in summer (JJA) in northwest India (D&W) and East Asia, the greater the likelihood of a stronger heat wave occurrence. Figure 10b displays the relationship when the linear trend is removed for the period of 1979-2018. Cases from 1994 and 2018 still stay highest in the graph, but for 2018, both HWI and CGTI dropped a little and for 1994, both values rise. After detrending, the correlation coefficient decreased but a linear relationship between CGTI and HWI is still present. Notice that the CGT is stronger in 1994 than in 2018. This suggests that the reason for the most extreme heat waves in 2018 was due to warming effect as well as CGT. In addition, it is difficult to explain the presence of the wave-train associated with CGT over Northern Hemisphere only with the index. To verify the presence, at least five anticyclonic anomalies should show on the locations mentioned in Table 1 at 200-hPa geopotential height. The years in which the positive anomalies are found in all five regions are 1990, 1994, and 2018. The following is an explanation of the case of 1990, which is considered to be an exception. In the 1990s, which ranked 5th during the 40 years (Fig. 2), the 200-hPa geopotential height anomaly patterns in mid-latitude are similar to CGT. However, the CGT pattern was prominent in August, not in July. Heat event occurs more in August, which is consistent with

the greater intensity of the CGT pattern in August (Fig. 11). Therefore, the fact that the CGTI is highly correlated with the intensity of the heat waves is still valid. Hence, the case of 1990 also supports the relationship between CGTI and heat wave.

The heat waves that occurred in 1994 and 2018 were caused by the early end of the Changma, the northward shift of jet stream, barotropic anomalous high over South Korea because of ISM and CGT, and its' stagnation. We defined heat waves with these four characteristics as CGT type heatwave.

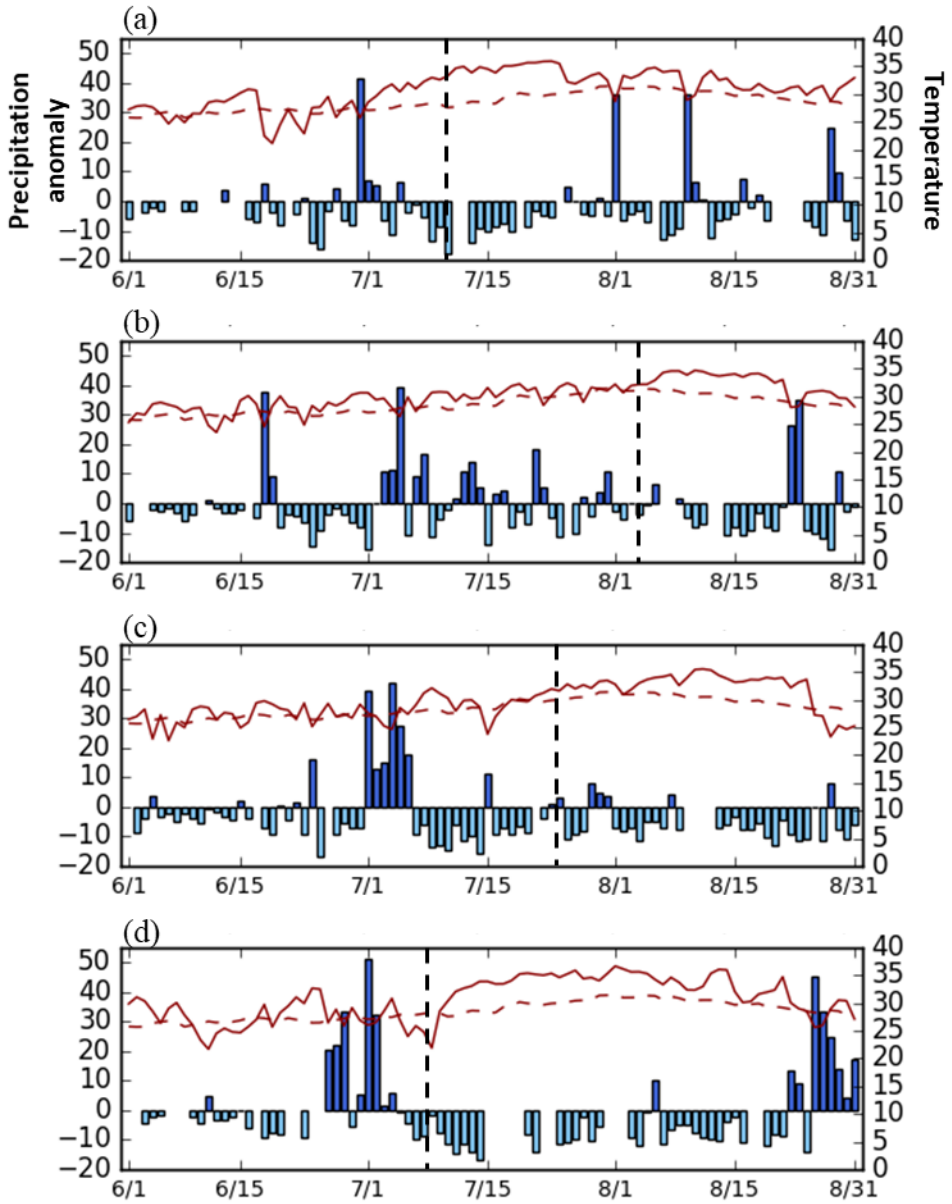

Figure 4. Precipitation anomaly (mm) and maximum temperature (° C) in (a) 1994, (b) 2013, (c) 2016 and (d) 2018. The bar denotes precipitation anomaly. The red solid line denotes daily maximum temperature, and the red dashed line denotes climatology for 1979–2018. The black dashed line denotes Changma retreat date.

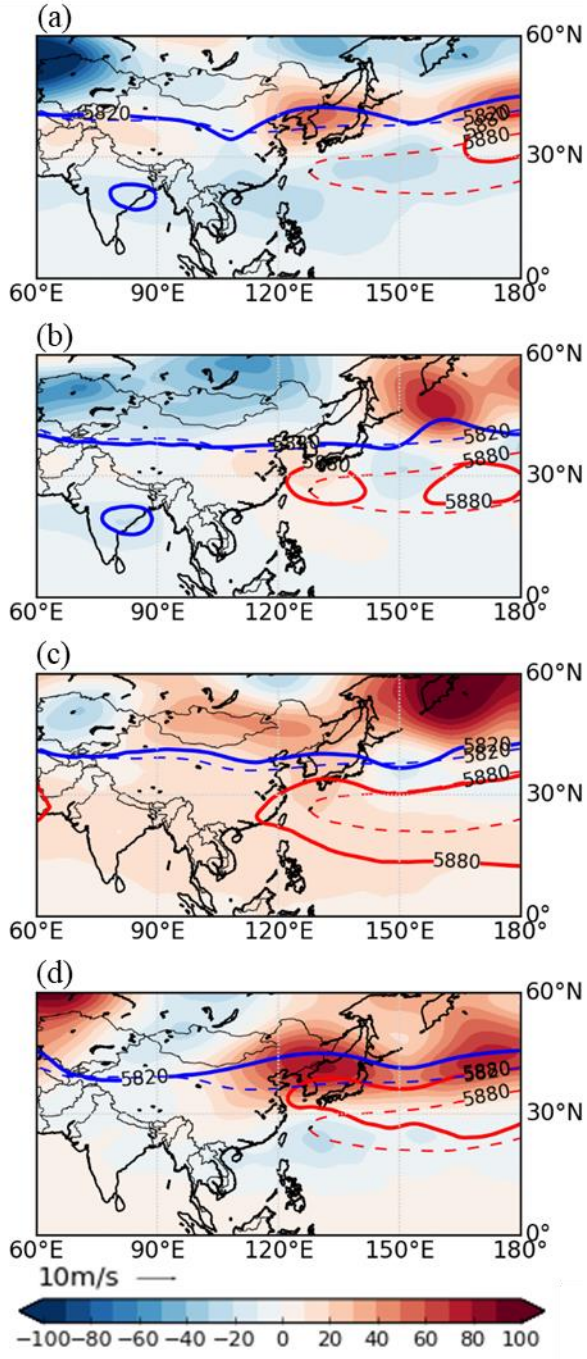

Figure 5. Composite anomalies of geopotential height at 500-hPa (shading, m), zonal and horizontal winds (vector, m s^{-1}) during July in (a) 1994, (b) 2013, (c) 2016 and (d) 2018. The blue(red) lines denote the 5820 m (5880 m) for geopotential height at 500-hPa.

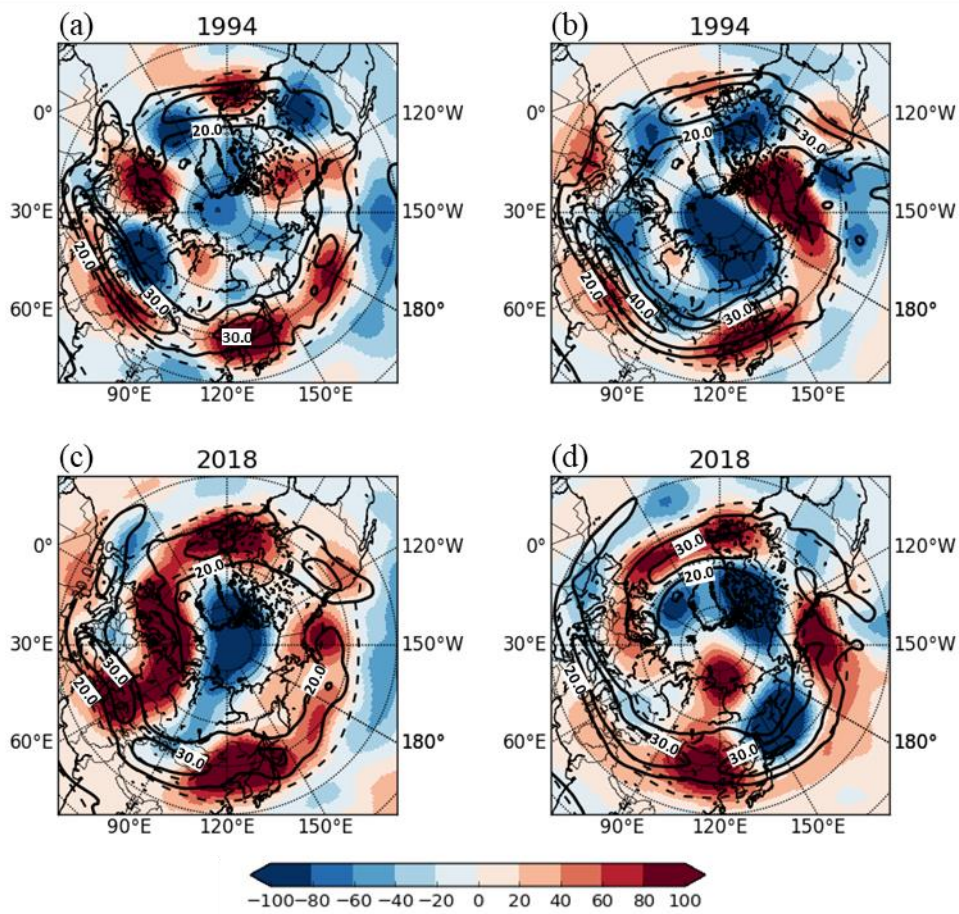

Figure 6. Composite anomalies of geopotential height at 200-hPa (shading, m) and wind speed (contour, m s^{-1}) during July (left panels) and August (right panels) in (a-b) 1994, and (c-d) 2018.

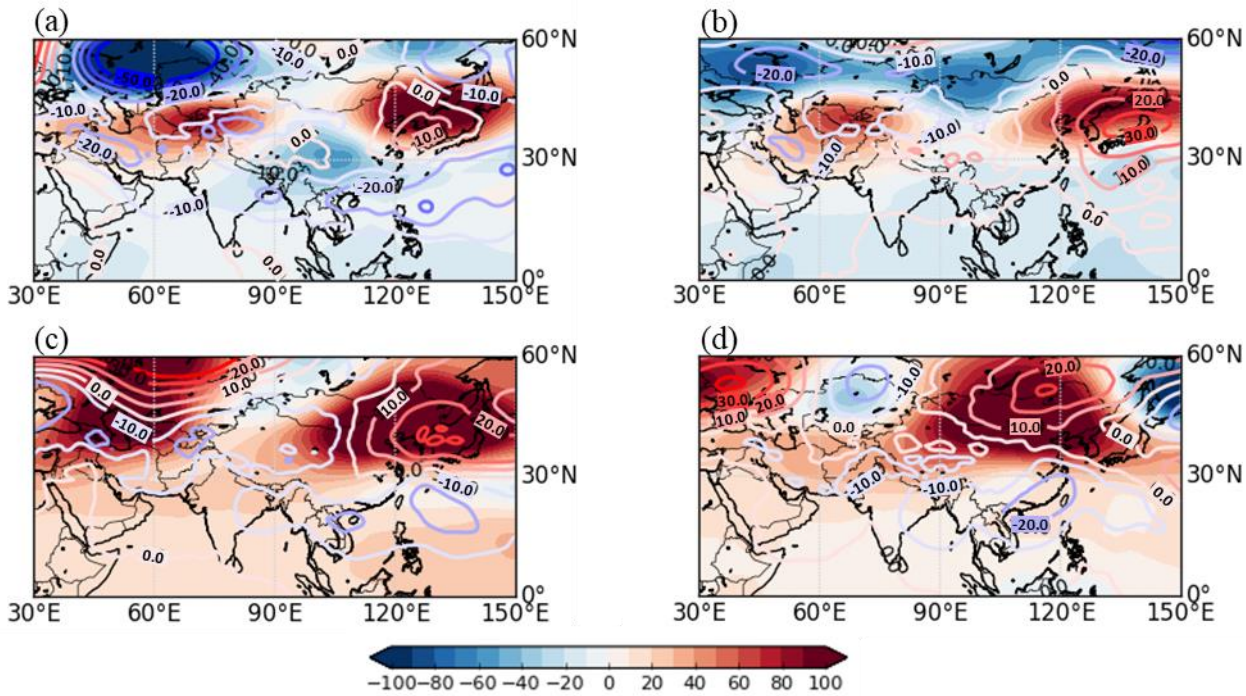

Figure 7. Composite anomalies of geopotential height at 200−hPa (shading, m) and at 850−hPa (contour, m) during July (left panels) and August (right panels) in (a, b) 1994 and (c, d) 2018.

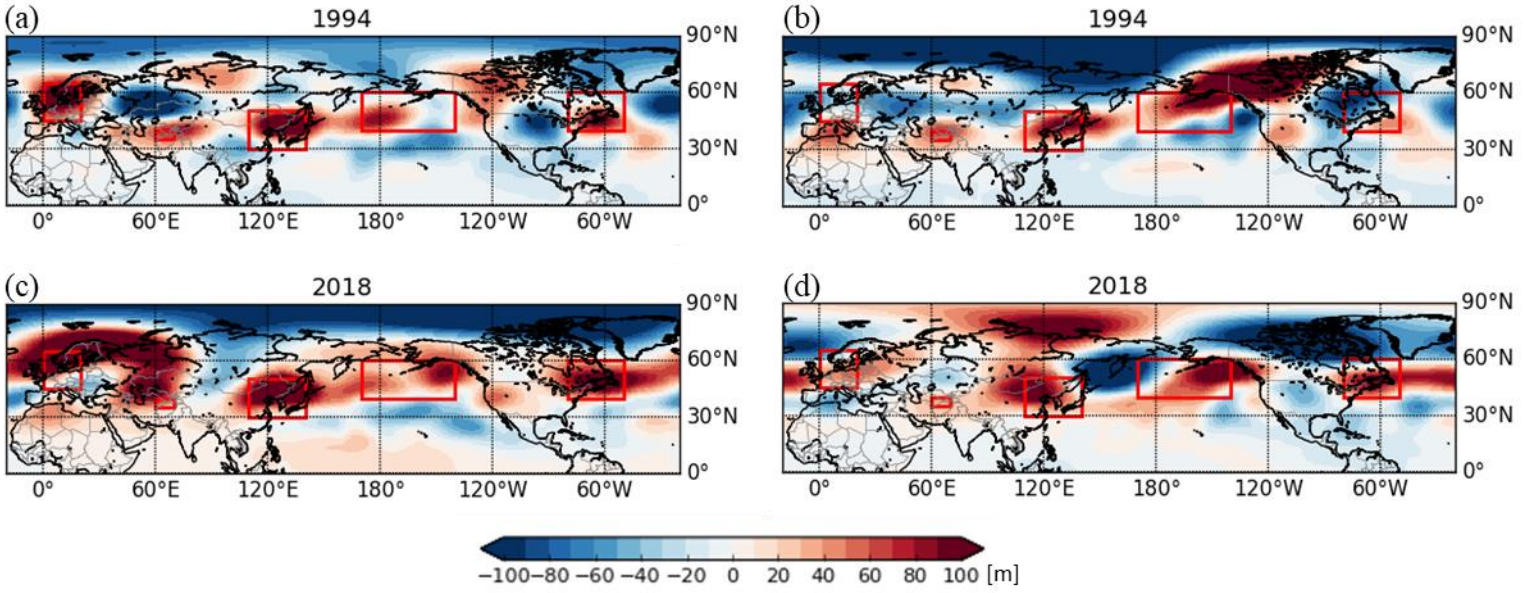

Figure 8. Composite anomalies of detrended geopotential height at 200−hPa (shading, m) during July (left panels) and August (right panels) in (a−b) 1994 and (c−d) 2018. The boxes indicate the regions defined as the CGT centers.

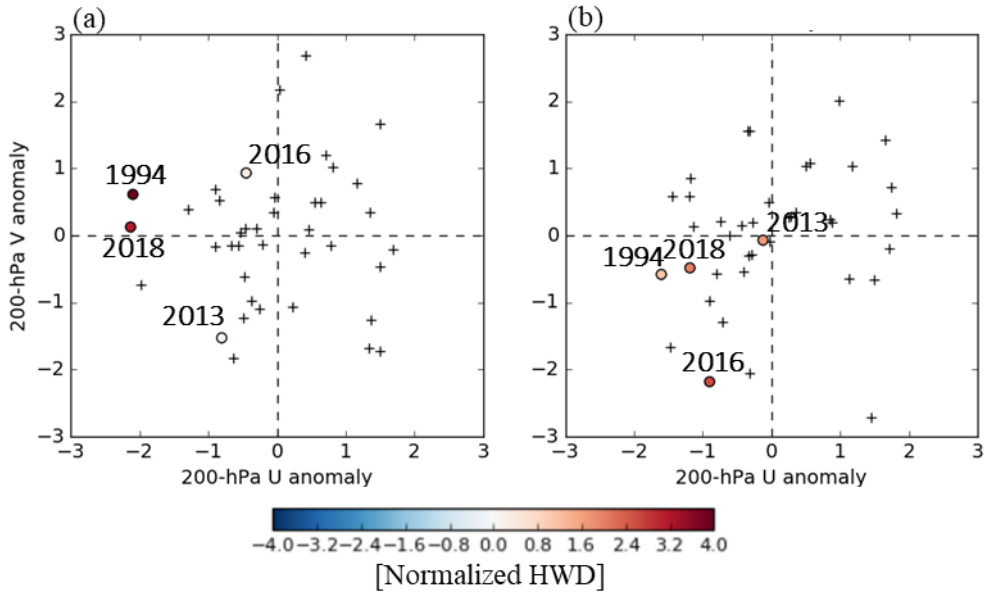

Figure 9. Normalized zonal and meridional wind anomalies in KP region in (a) July and (b) August. The dots represent the normalized monthly heat wave days.

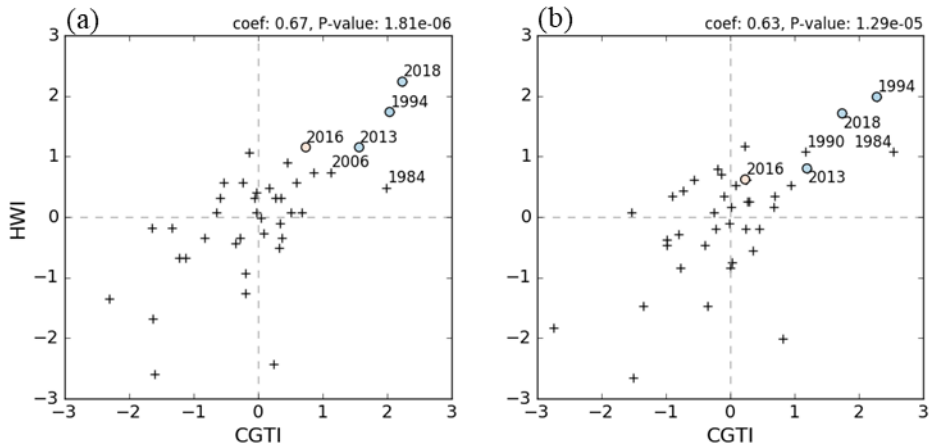

Figure 10. Relationship between normalized CGT index and the intensity of heat waves. (b) is the same as (a) except it is detrended.

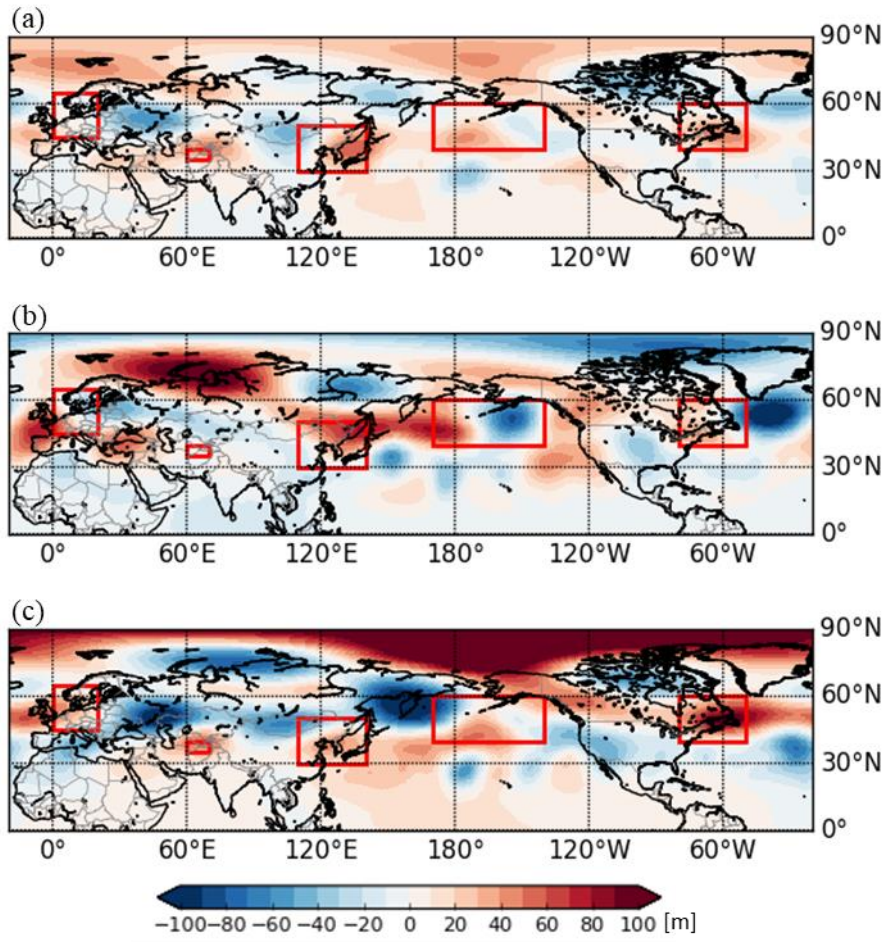

Figure 11. Composite anomalies of detrended geopotential height at 200-hPa (shading, m) during (a) summer (JJA), (b) July and (c) August in 1990. The boxes indicate the regions defined as the CGT centers.

4.2 Warm advection type

To identify the physical mechanism associated with the heatwaves in 2013 and 2016, the same variables that were mentioned in the 4.1 section were analyzed. In 2013 (Fig. 4b) and 2016 (Fig. 4c), the Changma retreat date is little later or similar to climatology, hence the precipitation is often observed in July, and the maximum temperature increases after Changma ends. The reason for this would be the strong strength of polar air mass despite the expansion of the North Pacific high (Fig 5b and c) which is related with AO. The normalized summer AO index in 2013 and 2016 is 0.66 and 0.81, respectively (Table 3). Compared to the AO index of 1994 and 2018, the AO index of 2013 and 2016 is lower. It can be expected that the geopotential height over the Arctic would be relatively high and therefore jet stream would not be able to shift much northward because of the weakened northward meridional wind. This expectation is well presented in Figure 12. The geopotential height over Arctic has positive anomalies in July 2013 (Fig. 12a). There is not much difference in geopotential height between mid- and high-latitudes (Fig. 12b and c). In addition, the jet stream near the Korean Peninsula is almost the same as the climatology except August 2016. However, unlike the 1994 and 2018 heatwaves, the cases of 2013 and 2016 have been extreme starting from August, and the characteristics of the August heat wave cannot be explained by the AO index.

The normalized ISM index shows a strong Indian monsoon with 2.69, 1.48 in the summer of 2013 and 2016 (Table 3). The composite map of geopotential height anomalies at 200-hPa and 850-hPa are shown in Figure 13. In the case of 2013, there are strong negative anomalies near the India continent in July. In addition, there is an anomalous high in the lower and upper troposphere near the Korea Peninsula, while the lower part is located in the south of the Korean Peninsula (Fig. 13a). The positive anomalies located in the south of the peninsula would continue to supply hot and humid air to Korea which suggested the longer Changma. In August, dipole pattern exists in East Asia at 850-hPa, unlike 1994 and 2018 cases which rather showed barotropic high pressure system (Fig. 13b). Even though the ISM index in summer 2016 is high, ISM is not related to the occurrence of heatwaves in July and August, as the negative anomalies over India do not appear in July and August (Fig. 13c and d). Moreover, it is important to look at the anomalous low of August 2016 at 850-hPa over East Asia.

To identify the relationship between CGT pattern and heat wave in 2013 and 2016, figure 14 shows the 200-hPa geopotential height anomalies in the Northern Hemisphere. Even though the position of the anticyclonic anomalies in 2013 seems to be similar to that of the CGT pattern, there is an anomalous high geopotential height over Kamchatka Peninsula, which shows a slightly different mechanism from the above two years (Fig. 14a). In July 2016, the

positive anomalies over EA are irrelevant to the CGT pattern because of the negative anomalies in NWEUR and NAM (Fig. 14c). The westerly wind anomalies have week negative value in 2013 and 2016 compared to those of 1994 and 2018. However, meridional wind anomalies in 2013 have negative, and those in 2016 have positive (Fig. 9a). The fact that northward meridional wind has weakened seems to delay Changma retreat date. In August 2013 and 2016, the CGT pattern does not appear with increasing heat wave explaining that there was no relationship in this particular year between CGT and heat wave. (Fig. 14b and d).

Since the mechanisms of these two cases are not fully explained by the variables analyzed above, it is suggested that the mechanism is different from the cases of 1994 and 2018. In 2013, it shows the dipole pattern with negative anomalies over northeastern KP and positive anomalies over southwestern KP (Fig. 13b). Similarly, in 2016, there is positive anomalies over Mongolia and negative anomalies over southeastern KP as the dipole pattern (Fig. 13d). In these two years, KP region is located on the edge of negative anomalies at 850-hPa. Based on the fact that winds blow towards the low atmospheric pressure, we looked at the heat and moisture advection in the Korean Peninsula. Figure 15 shows the heat and moisture advection around the Korean Peninsula in August.

In 2013, hot and humid air from East China flows into South Korea (Fig. 15a and b). There is moisture in the air, which makes summer more humid. The anomalous dry and hot air in the east of

Mongolia enters South Korea from the northwest which heats the country in August 2016 (Fig. 15c and d). The incoming hot air cannot easily escape because of the strong anomalies in the Kamchatka Peninsula. In addition, these strong anomalies can cause easterlies which crosses the Taebaek Mountains, a mountain range that stretches across South Korea, resulting in foehn effect, which increases the temperature in the western Korean Peninsula. When rising air parcel reaches the condensation level, water vapor in the air parcel will begin condensing, and forming cloud droplets. To explain the case of 2016, with dry air introduced, high condensation height level, strong ascending air could not form rain droplets. As a result, heat waves were not solved by rain and remained. Figure 16, on the other hand, shows temperature and moisture advection in 1994 and 2018, which were previously classified as CGT types. In these two cases, advection is directed from KP area and out.

To numerically identify the advection entering South Korea, anomalies of 850-hPa and 1000-hPa geopotential height, specific humidity and 2m temperature and vertical velocity were calculated (Table 4). W sign indicates the inflow of hot air compared to normal years, and if there is more (less) moisture than normal in the air, it is indicated as H (D) marker. It is evident that moist (dry) and warm air enters the KP region from the third (second) quadrant in 2013 (2016). In addition, the updraft appears at 1000-hPa, and the downdraft is observed at 850-hPa. This indicates that the ascending air current is not strong compared with those of 2016. Of

the 40-year analysis period, there are 19 yearly cases when the negative anomalies are at the low level (850-hPa and 1000-hPa) in August in KP area. Among them, the year when the warm advection swept into the KP area is only six years. Of the six years, there are five years (1990, 2004, 2013, 2016 and 2017) when the HWD of August is higher than climatology. In 1998, the HWD was not higher than climatology because the incoming humid air was replaced by precipitation, which allowed heat to dissipate. Table 5 shows the 850-hPa geopotential height anomalies, the advection sign, heatwave days, and precipitation anomalies of the warm advection years except for 2013 and 2016.

Hence, warm advection type is defined when heat waves are caused by cyclonic anomalies over the KP as well as the incoming warm air to KP at lower troposphere.

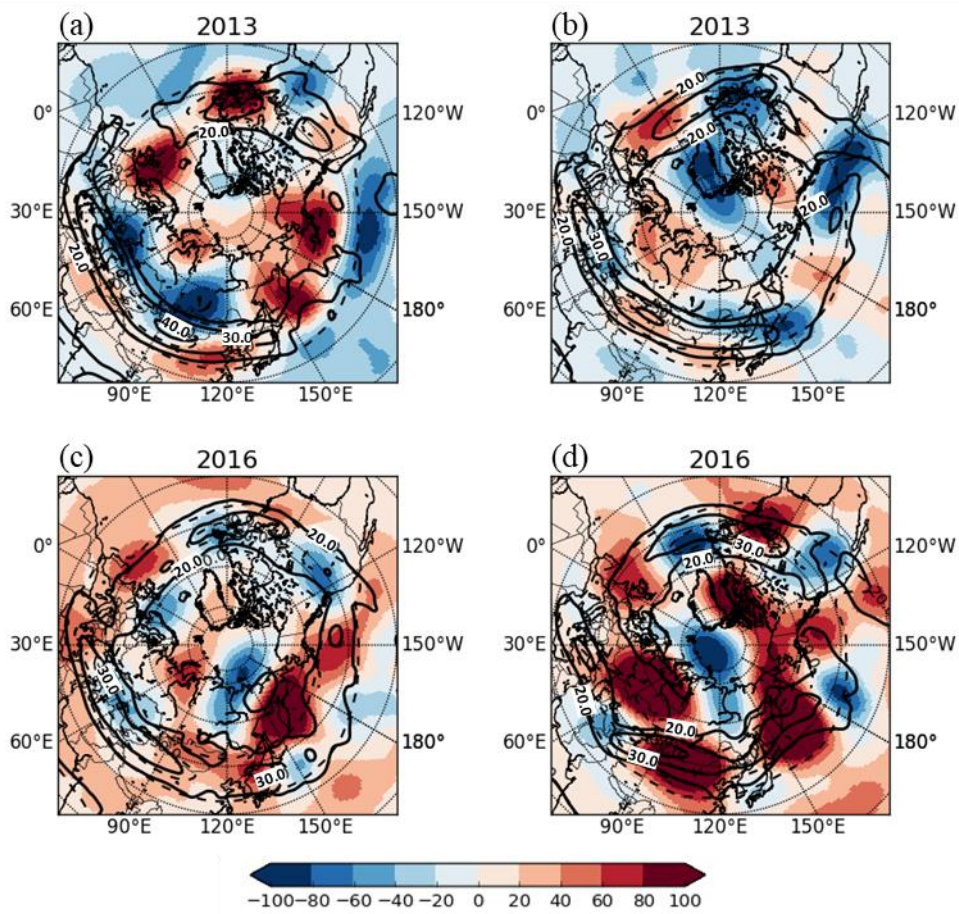

Figure 12. Same as Fig. 6 except for (a−b) 2013 and (c−d) 2016.

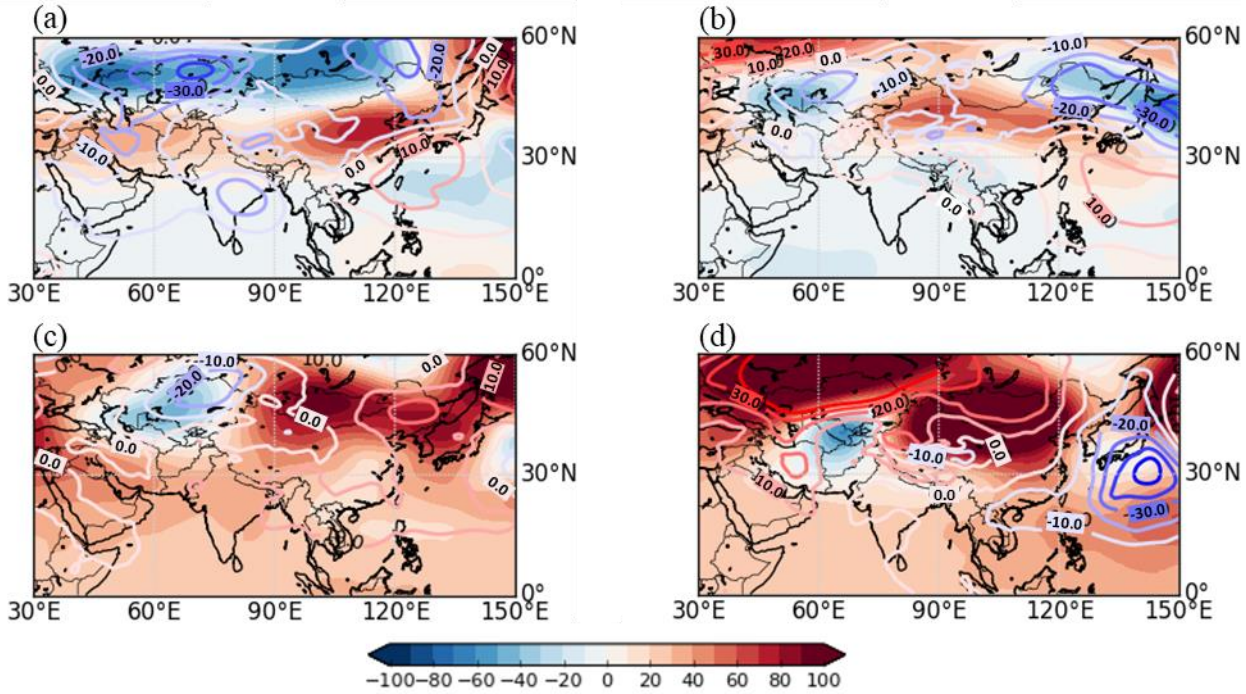

Figure 13. Same as Fig. 7 except for (a−b) 2013 and (c−d) 2016.

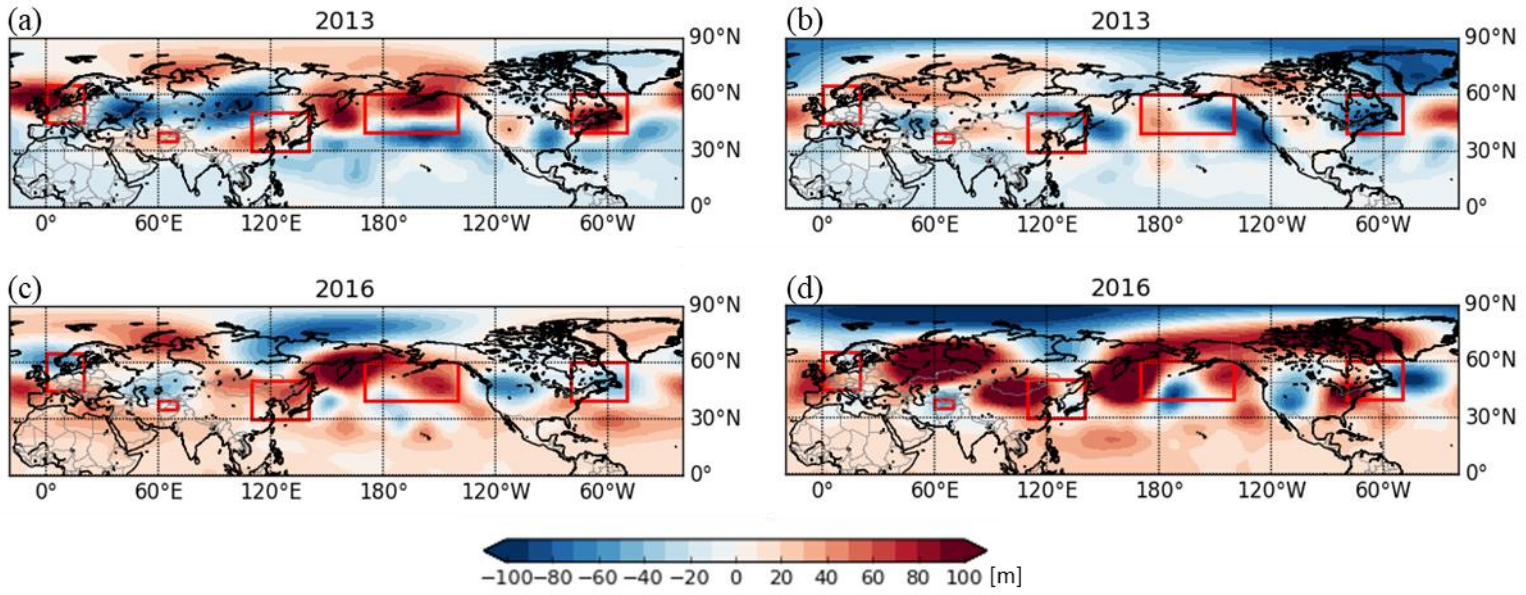

Figure 14. Same as Fig. 8 except for (a−b) 2013 and (c−d) 2016.

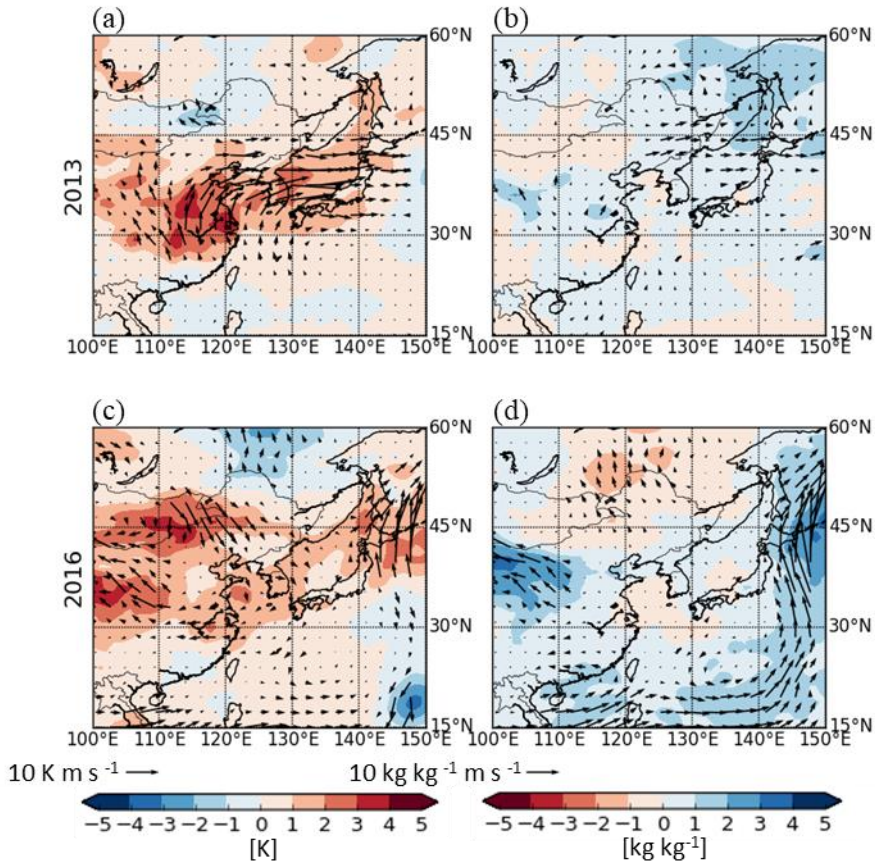

Figure 15. Composite anomalies of 2m temperature (shading, K; left panels) and specific humidity at 850-hPa (shading, kg kg^{-1}; right panels) during August of (a-b) 2013 and (c-d) 2016. The vectors indicate the advection of anomalous 2m temperature (K m s^{-1}) and anomalous specific humidity by submonthly wind (kg kg^{-1} m s^{-1}).

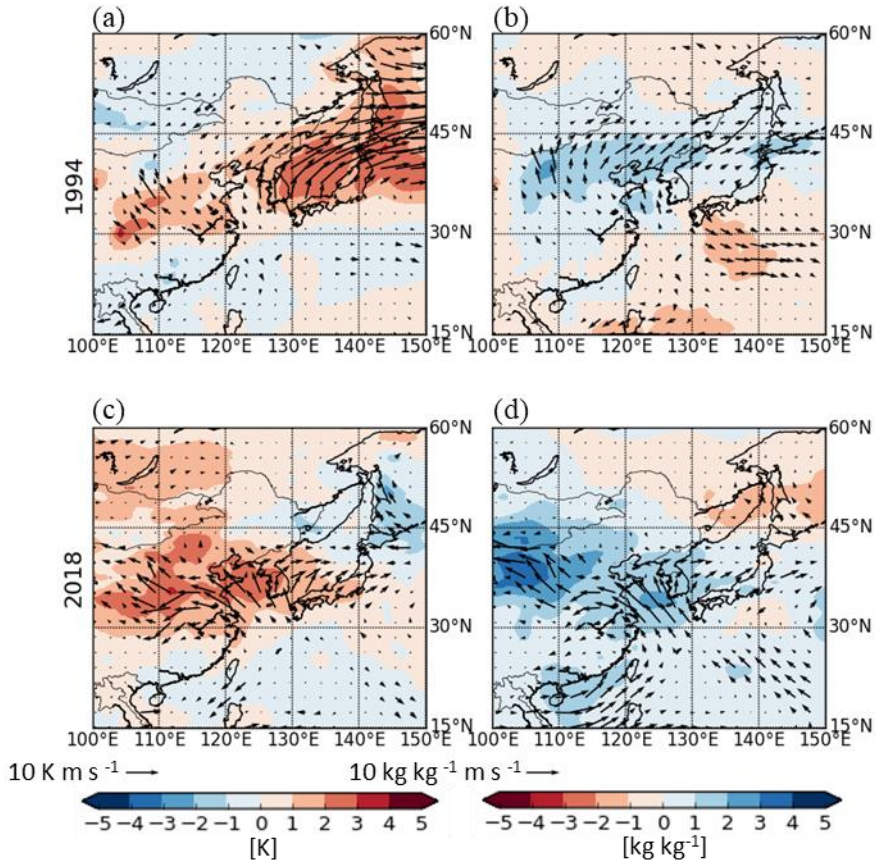

Figure 16. Same as Fig. 15 except for (a−b) 1994 and (c−d) 2018.

Table 4. Factors related to advection in August of 1994, 2013, 2016 and 2018. The first character in advection panels denotes presence or absence of warm advection. W represents heat advection existence. The second character (D or H) denotes whether or not there is a moist in the incoming air.

Year	HWD [days]	850−hPa geopotential height anomalies [m]	Advection				850−hPa vertical velocity [10^{-4} hPa s^{-1}]	LCL anomalies [m]
			1	2	3	4		
1994	10.4	24.89	·	·	·	WD	1.27	104.3
2013	13	−2.3	·	·	WH	·	2.14	79.1
2016	16.7	−15.39	·	WD	·	·	−0.5	161.8
2018	14.3	2.78	·	WH	·	WH	−1.35	137.1

1000−hPa geopotential height anomalies [m]	Advection				1000−hPa vertical velocity [10^{-4} hPa s^{-1}]
	1	2	3	4	
18.64	·	·	·	WD	−0.53
−11.56	·	·	·	·	−0.4
−21.67	WH	WD	·	·	−0.38
−5.88	·	·	·	WH	−0.56

Table 5. Factors related to advection in August 1990, 1998, 2004 and 2017. The first character in advection panels denotes presence or absence of warm advection. W represents heat advection existence. The second character (D or H) denotes whether or not there is a moist in the incoming air.

Years	850-hPa geopotential height anomalies [m]	Advection				HWD [days]	Precipitation Anomaly [mm]
		1	2	3	4		
1990	−2.87	·	·	·	WD	11.2	−1.05
1998	−1.55	·	·	WH	·	1.1	6.19
2004	−2.87	·	WD	·	·	8.4	1.84
2017	−4.68	·	WH	·	WH	5.8	−1.37

5. RCP8.5 projection of extreme heat waves

5.1 Circumglobal teleconnection type

In the future climate scenarios, we looked at how often CGT patterns would occur to understand the CGT type heat waves. CGT patterns were selected to assess future climate as it represents both prolonged barotropic high-pressure system and stagnated high-pressure system. Figure 17 shows the frequency of CGT pattern, which indicates how many years have positive anomalies in all CGT centers in a 30-year interval. The declining value of the mid-21st century seems to be caused by a change in the input data from the 2040s when simulating RCP 8.5 in CESM1 CAM5. The definition of the RCP8.5 is to reach 8.5 Wm^{-2} in 2100, therefore, we cut the data for period 2006-2035 (Early21C) and 2071-2100 (Late21C) to ignore the process of mid-21st century. In the early 21st Century, the number of CGT pattern frequency is about 7 years within the 30-year interval, while in the late 21st Century there are about 9 years during one 30-year interval. The fact that more CGT patterns appear in mid-latitude of the Northern Hemisphere suggests that there is a greater likelihood of a stagnant atmospheric system. In other words, there is a possibility that tall high cases like 1994 and 2018 occur more frequently. The change in the correlation between CGT and HWI is shown in Figure 18. Both figures display a high linear relationship between CGTI and

HWI for both periods (Early21C and Late21C) in the RCP8.5 scenarios. The R values are 0.57 and 0.72, respectively. Therefore, the increasing relevance of two indices suggests that the intensity of heat waves is stronger when the anomalous high in D&W region intensify.

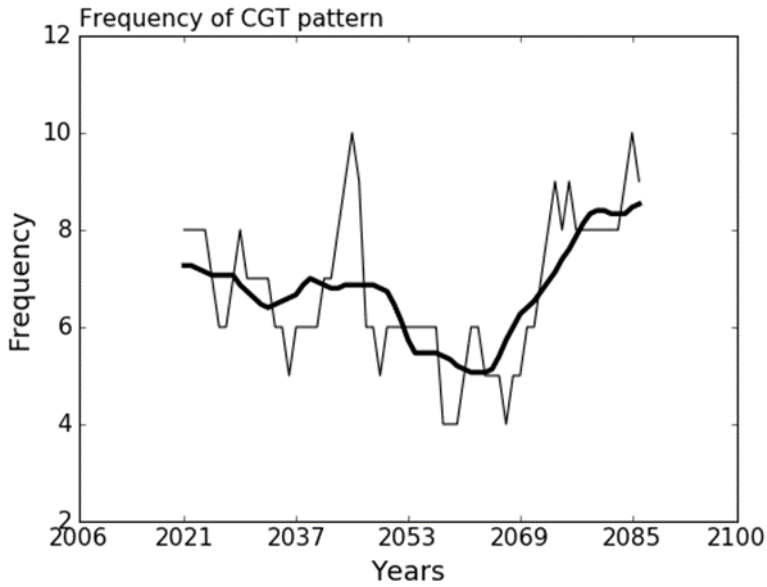

Figure 17. Time series of CGT pattern frequency from 2006–2100 with 30-year intervals (from 15 years before to 14 years after each year).

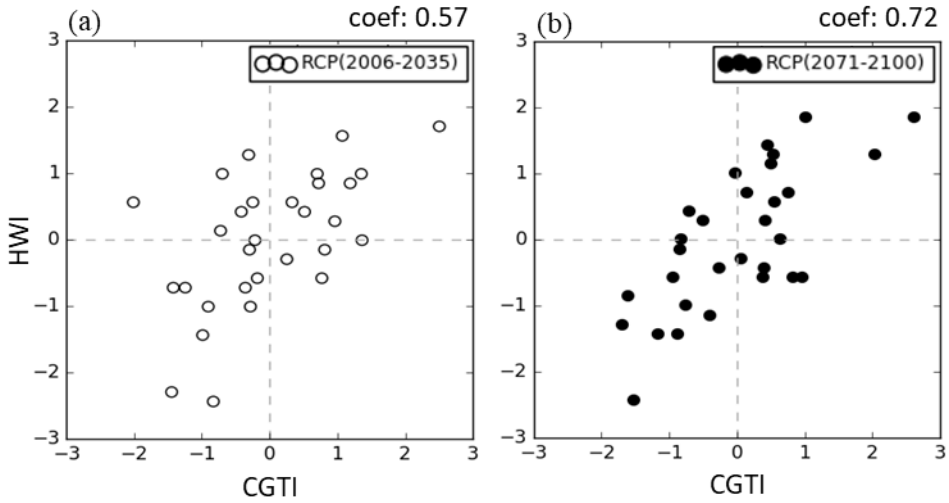

Figure 18. Same as Fig. 10b except for RCP8.5 scenario for the period (a) 2006–2035 and (b) 2071–2100.

5.2 Warm advection type

In order to know how much heat waves associated with heat and moisture advection in August will appear in the future scenario, we calculated 2m temperature anomaly and 850-hPa specific humidity in four numbered domains (Fig. 1b). Figure 19 shows the time series for the frequency of warming due to the advection induced by a low-level cyclone over 30 years while moving the analysis window. Advection from the first quadrant (green line) is not detected, and advection from the second quadrant appears two times during the 21st century (blue line). This flow appears only at Early21C and decreases with the latter half. In the case of the three quadrants (purple line) and the four quadrants (yellow line), most of the warm air entering the KP region comes from the south, which occurs about seven times and about four times in the 21C period, respectively. Similar to case of the second quadrant, these flows also decrease over the distant future. It can be seen that the frequency of warm advection into KP areas decreases significantly in the Late21C compared to the Early21C. At the Early21C, there are six years in which the summer temperature is more than one standard deviation above normal value in the first 30-year interval (2006-2035), three years of which are related to the advection of low-level cyclone. On the other hand, in the Late21C, seven years of the 30-year periods (2071-2100) have more than one standard deviation in summer temperature than normal. Of the seven only

two years are seen as inflows from surroundings to KP region. This suggests that the importance of advection related to heat waves in summer decreases.

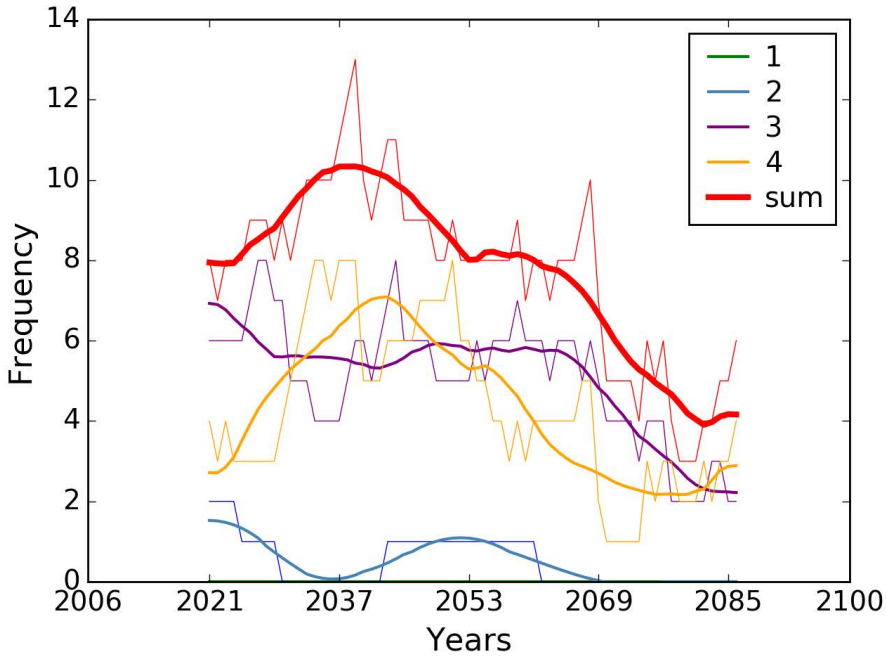

Figure 19. Time series of the frequency of heat advection in a moving 30-year window from 2006 to 2100. The green, blue, purple and yellow lines denote the advection from the first, second, third and fourth quadrant (Fig. 1b), respectively. The red line denotes the number of years in which advection from any quadrants appears during the 30-year period.

6. Discussion and Summary

In this study, we investigated the two dominant mechanisms that led to the heat waves in South Korea in 1994, 2013, 2016 and 2018. It was found that the factors affecting the heat waves of each months were different. The four cases were grouped in two: First, 1994 and 2018 with a large impact in July, and second, 2013 and 2016 with a large impact in August, according to the number of monthly heat wave days. To identify the mechanism of the occurrence of the four extreme heatwave cases, we examined Changma, the Arctic Oscillation, Indian summer monsoon, and CGT, which are directly correlated with the heatwave days among the climatic factors related to the heat wave in Korea. Early withdrawal of Changma, anticyclonic blocking and sinking motions associated with CGT play a role to induce the heat wave in July. Therefore, this heatwave is defined as the CGT type heat wave. In August, the heat advection from surroundings of the lower troposphere is important, which is called warm advection type heatwaves. Looking at the changes in these factors in the future climate, the number of CGT outbreaks in the Northern Hemisphere would occur more often in the distant future and showed a tight relationship with the heat wave intensity in South Korea. On the other hand, it was found that the frequency of heat advection in August would decrease over the last half of the 21st century.

For CGT type, in 1994 and 2018, the heat waves became worse

as the Changma ended early in July. On top of that, anticyclone related to CGT pattern had been located on the Korean Peninsula, further strengthening the heat waves. The process of occurrence of the CGT pattern is as follows. The energy created by the strong convection in India is transmitted to East Asia through the upper-level northwest of India by the Rossby wave, and the high pressure that induces the downdraft is created (Ding and Wang, 2005). When five anticyclonic anomalies like wave trains are created from East Asia to the North Pacific, North America, and Europe, the mid-latitude air circulation is stabilized and the atmosphere is stagnant. Thus, the airflow in East Asia is stagnated and continues to maintain the anticyclonic anomaly until August. Similar cases appeared in 1990, having strong CGTI in August rather than in July. Correspondingly the increase in the number of heat wave days occurred in August.

As warm advection type, the heat waves in 2013 and 2016 were linked to the heat advection into the Korean Peninsula. The signs of cyclonic anomalies at the bottom of the Korean Peninsula indicate the possibility of air flowing in from the surrounding area. In 2013, warm and humid air from Eastern China moved toward the low-pressure center in the northeastern part of the Korean peninsula, affecting South Korea. At this time, some downward flow on the KP region left the hot air on the lower floors. The 2016 case was a little different. The hot and dry air from the strong anticyclonic anomaly in Mongolia flew into the Korean Peninsula and

it could not escape easily due to the strong positive anomaly of the Kamchatka area. The rising air was dry, so it did not make precipitation and served to heat it up even more. Strong positive anomalies in Mongolia and the Kamchatka Peninsula correlates with CGT. In addition, anomalous high geopotential height in the Kamchatka region is significantly associated with the western–to–central subtropical Pacific (Yeh et al., 2018).

The likelihood of CGT's occurrence would increase in the distant future in RCP8.5 scenarios. Moreover, it would become more closely linked to the heat wave intensity in the summer of the Korean Peninsula. Surprisingly, the possibility of heat advection from nearby areas would decrease. This suggested that the impact of nearby areas is getting less and less, and the importance of remote connections across the mid–latitude area becomes greater., The mechanisms that produce these results have not been addressed, which requires further study. There exists a methodological limitation that the CGT center set based on the observation results can change in the future.

In order to know the future change of heat waves in South Korea, we need to understand the current heat wave. The analysis of the exceptionally severe heatwave cases allows us to anticipate and prepare for similar heatwaves. In this respect, this study will help to better understand which mechanisms mainly cause the heatwaves in South Korea and to increase the prediction capability of hot days in the future.

Reference

Alexander, L. V., Zhang, X., Peterson, T. C., Caesar, J., Gleason, B., Klein Tank, A. M. G., ... Vazquez-Aguirre, J. L. (2006) Global observed changes in daily climate extremes of temperature and precipitation. *Journal of Geophysical Research: Atmospheres*, **111**(D5).

Amengual, A., Homar, V., Romero, R., Brooks, H. E., Ramis, C., Gordaliza, M., & Alonso, S. (2014) Projections of heat waves with high impact on human health in Europe. *Global and Planetary Change*, **119**, 71–84.

Beniston, M., Stephenson, D. B., Christensen, O. B., Ferro, C. A. T., Frei, C., Goyette, S., ... Woth, K. (2007) Future extreme events in European climate: an exploration of regional climate model projections. *Climatic Change*, **81**(1), 71–95.

Beverley, J. D., Woolnough, S. J., Baker, L. H., Johnson, S. J., & Weisheimer, A. (2019) The northern hemisphere circumglobal teleconnection in a seasonal forecast model and its relationship to European summer forecast skill. *Climate Dynamics*, **52**(5), 3759–3771.

Korea Meteorological Administration. (2011) White paper on Changma, *Korea Meteorological Administration*, 12–42.

Duan, A. M., & Wu, G. X. (2005) Role of the Tibetan Plateau thermal forcing in the summer climate patterns over subtropical Asia. *Climate Dynamics*, **24**(7), 793–807.

Ding, Q., & Wang, B. (2005) Circumglobal Teleconnection in the Northern Hemisphere Summer. *Journal of Climate*, **18**(17), 3483–3505.

Ding, Q., & Wang, B. (2007) Intraseasonal teleconnection between the Eurasian wave train and the Indian monsoon. *Journal of Climate*, **20**, 3751–3767.

Frich, P., Alexander, L. V., Della-Marta, P., Gleason, B., Haylock, M., Tank, A. M. G. K., & Peterson, T. (2002) Observed coherent changes in climatic extremes during the second half of

the twentieth century. *Climate Research*, **19**(3), 193–212.

Ha, K. J., Chu, J. E., Lee, J. Y., Wang, B., Hameed, S. N., & Watanabe, M. (2012) What caused the cool summer over northern Central Asia, East Asia and central North America during 2009?. *Environmental Research Letters*, **7**(4), 044015.

Ham, Y. G., Kug, J. S., Yeh, S. W., & Kwon, M. (2016) Impact of two distinct teleconnection patterns induced by western Central Pacific SST anomalies on Korean temperature variability during the early boreal summer. *Journal of Climate*, **29**(2), 743–759.

Kim, C. G., Lee, S. M., Jeong, H. K., Jang, J. K., Kim, Y. H., & Lee, C. K., (2010) Impacts of Climate Change on Korean Agriculture and Its Counterstrategies. *Korea Rural Economics Institute*, **306**.

Kysely, J., & Kim, J. (2009) Mortality during heat waves in South Korea, 1991 to 2005: how exceptional was the 1994 heat wave?. *Climate research*, **38**(2), 105–116.

Lau, K. M., Lee, J. Y., Kim, K. M., & Kang, I. S. (2004) The North Pacific as a regulator of summertime climate over Eurasia and North America. *Journal of Climate*, **17**(4), 819–833.

Lee, J. Y., Wang, B., Ding, Q., Ha, K. J., Ahn, J. B., Kumar, A., ... & Alves, O. (2011) How predictable is the northern hemisphere summer upper-tropospheric circulation?. *Climate dynamics*, **37**(5–6), 1189–1203.

Lee, J.-Y. (2018) Interdecadal Changes in the Boreal Summer Tropical-Extratropical Teleconnections Occurred Around Mid-to-late 1990s. *Atmosphere*, **28**, 325–336 (in Korean with English abstract)

Lee, S.-S., Seo, Y.-W., Ha, K.-J., & Jhun, J.-G. (2013) Impact of the western North Pacific subtropical high on the East Asian monsoon precipitation and the Indian Ocean precipitation in the boreal summertime. *Asia-Pacific Journal of Atmospheric Sciences*, **49**(2), 171–182.

Lee, W.-S., & Lee, M.-I. (2016) Interannual variability of heat waves in South Korea and their connection with large-scale atmospheric circulation patterns. *International Journal of Climatology*, **36**(15), 4815–4830.

Lee, W. K., Lee, H. A., Lim, Y. H., & Park, H. (2016) Added effect of heat wave on mortality in Seoul, Korea. *International Journal of Biometeorology*, **60**, 719–726.

Lhotka, O., & Kyselý, J. (2015) Characterizing joint effects of spatial extent, temperature magnitude and duration of heat waves and cold spells over Central Europe. *International Journal of Climatology*, **35**(7), 1232–1244.

Meehl, G. A., & Tebaldi, C. (2004) More Intense, More Frequent, and Longer Lasting Heat Waves in the 21st Century. *Science*, **305**(5686), 994–997.

Min, S., Kim, Y., Kim, M., & Park, C. (2014) ASSESSING HUMAN CONTRIBUTION TO THE SUMMER 2013 KOREAN HEAT WAVE. *Bulletin of the American Meteorological Society*, **95**(9), S48–S51.

Raman, CRV, & Rao, YP (1981) Blocking highs over Asia and monsoon droughts over India. *Nature*, **289**, 271–273

Sobel, A. H., & Camargo, S. J. (2005) Influence of western North Pacific tropical cyclones on their large-scale environment. *Journal of the atmospheric sciences*, **62**(9), 3396–3407.

Sui, C. H., Chung, P. H., & Li, T. (2007) Interannual and interdecadal variability of the summertime western North Pacific subtropical high. *Geophysical Research Letters*, **34**(11).

Thompson, D. W., & Wallace, J. M. (2000) Annular modes in the extratropical circulation. Part I: Month-to-month variability. *Journal of climate*, **13**(5), 1000–1016.

Wang, B., & Fan, Z. (1999) Choice of South Asian summer monsoon indices. *Bulletin of the American Meteorological Society*, **80**(4), 629–638.

Wang, B., Wu, R., Lau, K.-M., (2001) Interannual variability of Asian summer monsoon: Contrast between the Indian and western North Pacific-East Asian monsoons. *Journal of climate*, **14**, 4073–4090.

Wang, B., Bao, Q., Hoskins, B., Wu, G., & Liu, Y. (2008) Tibetan Plateau warming and precipitation changes in East Asia. *Geophysical Research Letters*, **35**(14).

Wang, B., Lee, J. Y., Kang, I. S., Shukla, J., Park, C. K., Kumar, A., ... & Zhou, T. (2009) Advance and prospectus of seasonal prediction: assessment of the APCC/CliPAS 14−model ensemble retrospective seasonal prediction (1980–2004). *Climate Dynamics*, **33**(1), 93–117.

WNO, (2019) WMO statement on the State of the Global Climate in 2018. *World Meteorological Organization*, 44pp.

Wu, R. (2017) Relationship between Indian and East Asian summer rainfall variations. *Advances in Atmospheric Sciences*, **34**(1), 4–15.

Xu, K., Lu, R., Kim, B.−J., Park, J.−K., Mao, J., Byon, J.−Y., ... Kim, E.−B. (2019) Large−Scale Circulation Anomalies Associated with Extreme Heat in South Korea and Southern–Central Japan. *Journal of Climate*, **32**(10), 2747–2759.

Yeh, S. W., Won, Y. J., Hong, J. S., Lee, K. J., Kwon, M., Seo, K. H., & Ham, Y. G. (2018) The record−breaking heat wave in 2016 over South Korea and its physical mechanism. *Monthly Weather Review*, **146**(5), 1463–1474.

Yeo, S. R., Yeh, S. W., Won, Y., Jo, H., & Kim, W. (2017) Distinct mechanisms of Korean surface temperature variability during early and late summer. *Journal of Geophysical Research: Atmospheres*, **122**(12), 6137–6151.

Yoo, S. H., Ho, C. H., Yang, S., Choi, H. J., & Jhun, J. G. (2004) Influences of tropical western and extratropical Pacific SST on East and Southeast Asian climate in the summers of 1993–94. *Journal of climate*, **17**(13), 2673–2687.

Zuo, J., Pullen, S., Palmer, J., Bennetts, H., Chileshe, N., & Ma, T. (2015) Impacts of heat waves and corresponding measures: a review. *Journal of Cleaner Production*, **92**, 1–12.

국문 초록

본 연구에서는 우리나라에서 발생한 극심한 폭염 사례를 두 가지 유형으로 구분하였다. 분석대상으로 선정한 해는 1994년, 2013년, 2016년, 그리고 2018년이며, 이 해들은 폭염 발생일이 40년 평균 (10.6 일)보다 1 표준편차 (6.9 일) 이상 되는 극심한 폭염이 발생한 해이다. 네 개의 해에서 나타난 폭염 발생 메커니즘을 분석하기 위하여, 우리나라 폭염과 관련된 기후 인자들 중 폭염 일과 상관성이 직접적으로 높은 북극진동, 인도 몬순, CGT (circumglobal tele-connection), 그리고 장마를 중심으로 살펴보았다. 첫번째로 1994년과 2018년 사례에서 나타나는 유형은 CGT 유형으로 7월부터 한국의 폭염이 심해지는 경우이다. CGT 유형에서 나타난 기후적 특징은 1) 장마의 조기 종료, 2) 북극의 평년보다 낮은 지위 고도로 인한 제트기류의 북상, 3) 강한 인도 몬순과 중위도 전역에 나타난 CGT 패턴으로 인한 키 큰 고기압 형성과 동서방향 대기 순환 정체이다. 우리나라에 키 큰 고압시스템이 쉽게 빠져나가지 못해 맑은 날씨와 하강 흐름이 만드는 지속적인 무더위가 CGT 유형 폭염의 특징이다. 두번째 유형은 8월부터 폭염이 심해지는 경우로 온난이류 유형이라 구분하며 2013년과 2016년 폭염 사례가 여기에 해당된다. 온난이류 유형에서 나타난 기후적 특징은 1) 한반도 하층에 저기압 존재, 2) 몽골 지역과 중국 화동 지역으로부터의 뜨거운 공기 유입이 있다. 주변 지역에서 생성된 뜨거운 공기가 한반도로 직접 유입되어 폭염을 발생 시킨다.

우리나라 폭염이 미래에 어떠한 형태를 갖는지 알기 위해서, RCP 8.5 시나리오에서 CGT 유형과 온난이류 유형의 미래 변화를 살펴보았

다. CGT 유형을 대표하는 CGT 패턴은 미래 기후 시나리오에서 먼 미래로 갈수록 발생 빈도가 증가하였고, 온난이류 유형은 점차 감소하였다. 이는 우리나라 폭염이 7월부터 강하게 나타나는 유형이 점차 많아지며 기후변화에 따른 폭염 심각성이 커질 수 있음을 암시한다.

주요어 : 폭염, CGT 패턴, 온난이류, 기후변화, RCP8.5 시나리오

학 번 : 2017-27486